Nano Energy 80 (2021) 105537

Contents lists available at ScienceDirect

Nano Energy

journal homepage: http://www.elsevier.com/locate/nanoen

Full paper

Fabrication of piezoresistive Si nanorod-based pressure sensor arrays: A promising candidate for portable breath monitoring devices

Ramesh Ghosh [a,*], Minho S. Song [a,b], JunBeom Park [a], Youngbin Tchoe [a,b], Puspendu Guha [b], Wanhee Lee [a], Yoonseo Lim [c], Bosung Kim [d], Sang-Woo Kim [d], Miyoung Kim [b,e], Gyu-Chul Yi [a,b,**]

[a] Department of Physics and Astronomy & Institute of Applied Physics, Seoul National University, Seoul 08826, South Korea
[b] Research Institute of Advanced Materials (RIAM), Seoul National University, Seoul 08826, South Korea
[c] Department of Materials, Imperial College London, London SW7 2BU, United Kingdom
[d] School of Advanced Materials Science and Engineering, Sungkyunkwan University (SKKU), Suwon 16419, South Korea
[e] Department of Material Science and Engineering, Seoul National University, Seoul 08826, South Korea

ARTICLE INFO

Keywords:
Si Nanorod
Piezoresistivity
Pressure sensor
Breath detection

ABSTRACT

This paper reports on the controlled fabrication of a highly sensitive piezoresistive sensor by using Si nanorod (NR) arrays. An efficient, large-area, scalable strategy was adopted to fabricate the pressure sensors by incorporating chemically etched, high-aspect-ratio, vertical Si NR arrays between two thin Au layers. The piezoresistive properties corresponding to dimension- and position-controlled and randomly etched, closely packed, and thin Si NR arrays were exploited to fabricate the small, portable, and device-compatible pressure sensors. The Si-NR-based piezoresistive sensors exhibited a high sensitivity of 0.49 MPa^{-1}, thereby demonstrating its superiority over other unconventional piezoresistive nanomaterials such as Si with different configurations of nanostructures. Furthermore, the sensors exhibited a large variation (~45%) in the current at a constant bias voltage of 2 V under a weak applied pressure corresponding to an inert gas flow of 5 sccm. The excellent pressure sensing performance of the piezoresistive Si NRs enabled the efficient detection of changes corresponding to the human breathing pattern. In particular, the key advantages of such pressure sensors is the simple, inexpensive, and scalable fabrication process; high sensitivity with ultra-low-pressure detection; and excellent ambient stability (>several months) with a high durability pertaining to more than 1,000 cycles of pressure loading/unloading. Furthermore, we demonstrated the ability of the pressure sensor to act as a portable human breath sensor to monitor respiratory parameters in a noninvasive and personalized manner. The results can provide direction for the realization of next-generation breath-sensing gadgets and other leading-edge applications in the domain of electronic and healthcare devices.

1. Introduction

Pressure sensors have attracted considerable interest owing to their potential for application in various areas including different industries, research domain, and environmental monitoring and human healthcare fields. Piezoresistivity plays a key role in the fabrication of high sensitivity, facile, and simple pressure sensors through different inorganic and organic materials in an inexpensive yet efficient manner [1–8]. Among the various material architectures, one-dimensional nanostructures, specifically, nanowires (NWs) and nanorods (NRs) are considered to be desirable for use in piezoresistive-based electronic devices [1,8]. Many researchers have investigated conventional piezoresistive nanomaterials such as ZnO, GaN, and CdS are extensively studied for utilizing their piezoresistive properties to develop high sensitivity pressure sensors [1,8–11]. Nevertheless, despite the extensive research efforts and certain notable advancements in the last two decades, to date, only a few pressure sensors have been practically implemented in healthcare devices. In general, most of the pressure sensors cannot be processed beyond the laboratory stage, as they cannot satisfy key requirements, such as a sufficient sensitivity and accuracy; low detection range; and high portability, reliability, and durability. Typically, portable and wearable pressure sensors are fabricated as

* Corresponding author.
** Corresponding author at: Department of Physics and Astronomy & Institute of Applied Physics, Seoul National University, Seoul 08826, South Korea.
E-mail addresses: Ramesh.Ghosh@glasgow.ac.uk (R. Ghosh), gcyi@snu.ac.kr (G.-C. Yi).

https://doi.org/10.1016/j.nanoen.2020.105537
Received 29 September 2020; Received in revised form 19 October 2020; Accepted 21 October 2020
Available online 27 October 2020

interlocked structures composed of composite polymers, such as polydimethylsiloxane (PDMS), combined with conductive active nanomaterials, such as metals, carbon nanotubes, reduced graphene oxide (rGO), and graphene [2–8,12–14]. These elastomer-based pressure sensors exhibit a high sensitivity, low detection limit, and rapid response, and can thus be utilized in piezoresistive electronic devices. However, the sensing performance of these composite elastomer-based piezoresistive pressure sensors is not satisfactory in long-term use as they are easily degraded in the ambient atmosphere. Furthermore, the elastomer-based portable and wearable pressure sensors are not suitable for application in high-resolution electronic skin devices, compared to the ordered arrays of vertically aligned NW/NR-based pressure sensors. Parallel to the piezoresistive pressure sensors, piezoelectric pressure sensors are also studied extensively where the material has inherent property to generate a spontaneous electrical signal when it is strained [15–20]. Unlike piezoresistive pressure sensors, piezoelectric pressure sensors do not require any external voltage source. If a voltage is applied in piezoelectric pressure sensors, the current induces a strain in material geometry which can also countable beside the external pressure-induced strain. Thus, piezoresistive pressure sensors are more preferable to detect dynamic changes in physical parameters like force, mass, flow, vibration etc [15]. Therefore, significant research attention needs to be required to examine the use of pressure sensors based on device-compatible piezoresistive nanomaterials to address the corresponding challenges in this domain. In this context, arrays of vertically aligned Si NWs/NRs are being considered the most promising candidate materials for developing piezoresistive pressure sensors. At present, nanostructured Si is the most widely used material in nanotechnology applications owing to its superior physical and chemical properties, eco-friendly nature, and high device compatibility [21–25]. Although the piezoresistive effect in Si NRs was observed almost a decade ago, only a few studies focused on examining the piezoresistivity of nanostructured Si have been reported [26–34]. According to the existing reports, the design of piezoresistive Si NR sensors is limited to the cantilever type, as it can efficiently detect the torque/force [26–29,34]. However, despite their superior mechanical and electrical properties, high-aspect-ratio Si NR arrays have not yet been applied in the design of pressure sensors that could be used in healthcare devices. In particular, to fabricate complementary metal–oxide–semiconductor (CMOS)-compatible air flow sensors, it is desirable to utilize the piezoresistive property of Si NRs to enable ultra-low-range pressure detection including that of air turbulence, human breathing, and acoustic vibrations in air [30].

In the last two decades, significant research has been performed to fabricate smart and portable sensors to monitor human breath [2–4,35,36]. In the conventional techniques to monitor human breath, the sensors operate based on different parameters such as the temperature, pressure, vibration, and chemical compounds sampled from the human breath (inhalation/exhalation). In addition, chemoresistive breath markers have been employed in novel medical diagnostic approaches, monitoring devices, and workout partner devices; however, their extensive utilization is restricted owing to the complexity of human breath, which may contain more than 800 compounds. In this regard, piezoresistive breath sensors composed of high-aspect Si NR arrays can be used to develop respiratory status monitoring devices to prevent breathing disorders such as sleep apnea in a simple, easy, and efficient manner.

Therefore, in this work, we demonstrated the bio-compatible, large-area, simple, rapid, scalable, and controlled fabrication of pressure sensors by using Si NR arrays. To fabricate the small, portable and device-compatible pressure sensors, the piezoresistive properties of close-packed, vertical, high-aspect-ratio Si NR arrays were exploited through dimension- and position-controlled etching as well as random etching processes. The prototype pressure sensors, which exhibited a high sensitivity and could realize ultra-low-pressure detection, were used as portable and wearable breath sensor to monitor the human respiratory parameters in a noninvasive and personalized manner.

2. Material and methods

2.1. Fabrication of the sensor devices

High-quality Si NR arrays were fabricated by a facile, scalable, and well-known metal-assisted chemical etching (MACE) method using Si wafers. Gold and silver were used as the noble metals and HF/H_2O_2 was used as the etchant to etch the *n*-type Si (100) wafers with a resistivity of 0.001 Ω-cm. Dimension- and position-controlled Si NRs were obtained through the selective and controlled etching of Si, and the respective samples were labeled as "NR_A". Specifically, a 15 nm-thick Au film with uniform hole array patterns of a controlled diameter and spacing was created on the Si wafer through e-beam lithography, and the Au-patterned Si wafers were etched in HF/H_2O_2 (8 M HF and 3 M H_2O_2). In general, the lateral dimension and spacing of the Si NRs depend upon the size and spacing of the Au hole array on Si, respectively, whereas the length depends on the etching duration. Thus, the diameter of the Si NRs was ensured to be in the range of 110–500 nm after removing the residual Au. Furthermore, large-area, close-packed Si NR arrays with a comparatively low but variable diameter were prepared through the Ag nanoparticle-assisted random etching of Si in HF/H_2O_2. The corresponding samples were labeled as "NR_B". Prior to etching, the Ag nanoparticles were coated on Si through a chemical process (in $HF/AgNO_3$ solution) [37]; the observed diameter of the Si NRs ranged from 20 nm to 120 nm. To fabricate the sensor devices, Au metal electrodes were deposited on the top (100 nm) and bottom (100 nm) sides of the Si NRs. Prior to the electrode deposition, the Si NR samples were treated with a buffered oxide etchant for 10 s to remove the surface native oxides.

2.2. Morphology and structural characterization

The morphology of the Si NR arrays was investigated using a field emission scanning electron microscope (FESEM, TESCAN) operated at 30 kV. Furthermore, this system was used to realize the e-beam lithography for the metal hole array and the examination of its morphology. The surface porosity of the Si NRs and formation of the Si nano-islands and crystal lattice fringes were studied using a field emission transmission electron microscope (analytical TEM, JEM-2100F, JEOL Ltd.). For this analysis, the Si NRs were scratched and dispersed in isopropanol and later drop-casted onto a lacey-carbon-coated Cu TEM grid.

2.3. Measurement of pressure response

2.3.1. Pressure application using a voice coil motor

The pressure sensing characteristics, i.e., the piezoresistive properties of the Si NRs were investigated by examining the current response under the impulse of a constant mechanical pressure. Specifically, mechanical force was applied to the sensor device via a sapphire stamp attached on the axis of a voice coil motor (VCM) tool, which generated force when placed in a magnetic field and subjected to an electric current. A controller was used to measure the applied force, with a precision of 0.001 N. A constant force, and thus, a constant pressure was applied throughout the experiment by using the force controller. The force was applied vertically to the surface of the sensor attached firmly on a flat surface. A smooth sapphire substrate (size: 9 mm^2) was placed between the VCM force application tip and the sensor to avoid the formation of unnecessary electrical pathways.

2.3.2. Pressure application using a constant flow of inert gas

A constant flow of inert gas, monitored by a mass flow controller (MFC), was used to impart uniform and constant pressure to the sensor. Two different inert gases, namely, nitrogen and argon, were used. The pressure sensor device was placed on a solid substance at a distance of 2 mm from the output of the MFC.

A variable bias voltage of − 2–2 V was applied to the device in both

the VCM and MFC cases via a source meter (Keithley-2601). The sensing performances of the prototype sensors were characterized by measuring the current–voltage (I–V) and current-time (I–T) curves during the presence/absence of pressure on the sensor.

3. Results and discussion

The surface morphology and the structure of the Si NR arrays prepared for the pressure sensors was investigated using the FESEM and TEM analyses as depicted in Fig. 1. Fig. 1(a) shows the 30° view of the dimension- and position-controlled Si NRs (NR_A) with a diameter of 500 nm, and Fig. 1(b) shows the cross-sectional FESEM images of the Si NRs prepared through Ag-assisted random etching of Si (NR_B). A diameter of up to 110 nm was attained for the uniform Si NRs through the Au-assisted controlled etching of Si. Fig. S1(a–c) and (d–f) show the NR_A samples of the Si NRs with a diameter of 110, 200, and 500 nm, etched for 5 and 10 min, respectively. When the diameter is 110 and 200 nm, the Si NRs appear to merge toward the top side and are elongated. Moreover, although Ag was used to fabricate the closely packed, thin Si NR arrays with a random size, the Si NRs prepared using the MACE technique are mesoporous, with the porosity depending on the etching parameters. Therefore, we tuned the porosity of the Si NRs by tuning the HF and H_2O_2 concentrations for the NR_B samples. The top- and cross-sectional-view FESEM micrographs of the Si NR arrays etched for 10 min under different HF and H_2O_2 concentrations are shown in Figs. S2 (a–d) and (e–h), respectively. The average diameter of the Si NRs in each case was < 50 nm, and the samples exhibited a variable length depending on the etchant concentration and etching duration. To investigate the surface properties of individual Si NRs, we examined the TEM analysis results of the as-prepared Si NR samples. The morphologies of the individual Si NRs are shown in Fig. 1(c–f). Fig. 1(c) shows the Si NRs extracted from an NR_A sample with a diameter of 500 nm, and Fig. 1(d) shows the Si NRs collected from the NR_B samples. The Si NRs in the NR_B samples exhibited a variable diameter ranging from 20 to 120 nm, with an average diameter of < 50 nm. The TEM images of the various Si NRs collected from the NR_B samples are shown in Figs. S3 (a–g). In all the etching scenarios, the Si NRs exhibited a mesoporous characteristic on their surfaces, which is in agreement with the previously reported findings [21,23,39]. The mesoporous nature of the Si NRs led to the formation of quantum-sized nano-islands on the Si NR surface. In addition, a short-range disorder in the atomic orientation was observed in the regions of the Si nano-islands, as reported in the literature [21,22,40–43]. The high-resolution TEM (HRTEM) images pertaining to the edge (Fig. 1(e)) and surface (Fig. 1(f)) confirmed the polycrystalline nature of Si in the region of the quantum-sized Si nano-islands. The size of the Si nano-islands was estimated considering the dotted lines (Fig. 1(f)), and the size was noted to be comparable or less than the excitonic Bohr diameter of Si (~9.8 nm). The selected area electron diffraction (SAED) pattern (inset of Fig. 1(e)) acquired from a single Si NR exhibited the polycrystalline nature of the Si nano-islands, even though the Si NRs were prepared from single-crystalline Si (100) wafer. Furthermore, the quantum-sized Si nano-islands corresponded to Si (111) planes, which is the orientation in which Si most effectively demonstrates piezoresistive properties [15,26,33]. The demonstration of piezoresistive properties is a key advantage of MACE-prepared Si NRs. In this configuration, the mechanically robust yet flexible, thin, and long Si NRs can exhibit sufficient potential to respond to a certain amount of applied pressure [29,30,38].

To fabricate the pressure sensor devices from the MACE-prepared Si NRs, a simple approach was adopted: a 100 nm-thick Au layer was deposited on each side of the Si NR samples. The fabrication steps of pressure sensors was schematically shown in Fig. 2 along with its FESEM

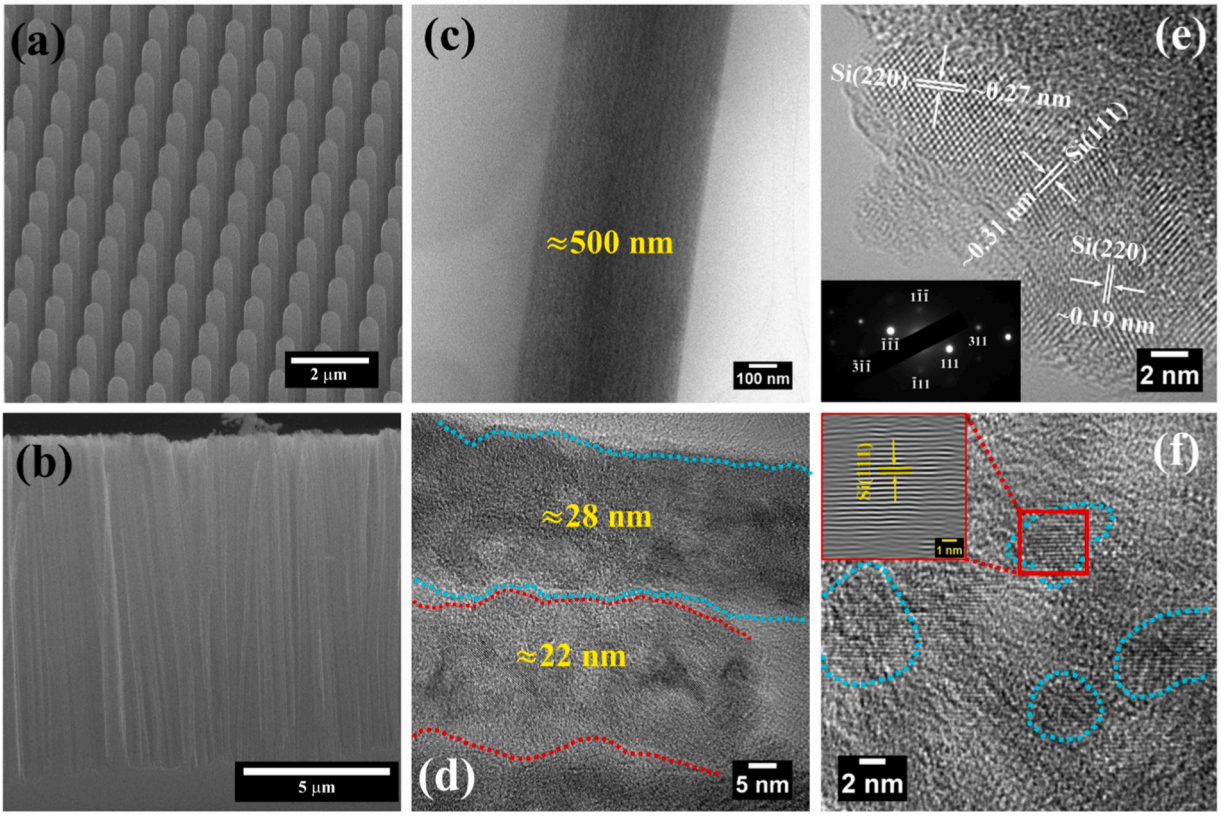

Fig. 1. (a) FESEM image (30° tilted) of the Si NR (diameter: 500 nm) arrays, NR_A. (b) FESEM image (cross-sectional) of the randomly etched Si NR (NR_B) arrays. (c, d) TEM image of the Si NRs collected from the NR_A and NR_B samples, respectively. HRTEM images pertaining to the (e) edge and (f) surface of an Si NR indicating the crystal planes with the dd-spacing. The size of the nano-islands is marked by dotted lines. SAED-pattern on a single Si NR is shown as an inset of (e).

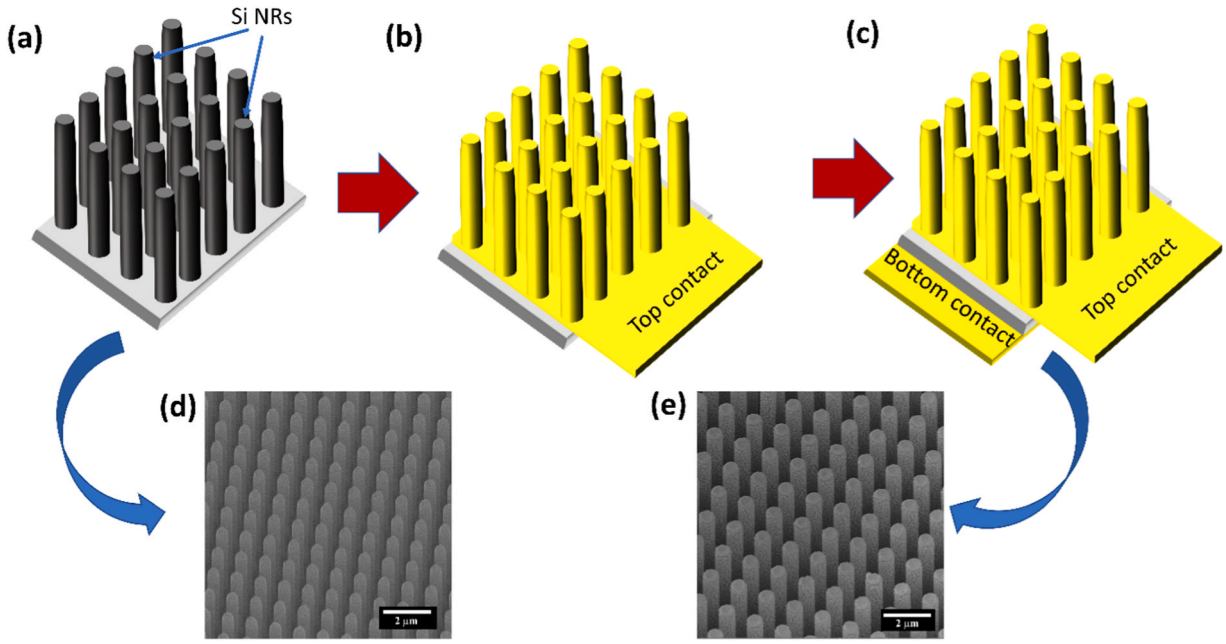

Fig. 2. (a–c) Schematic of the fabrication procedure of an Si NR-based pressure sensor. (d–e) FESEM image (30° tilted) of the Si NR (diameter 500 nm) arrays before and after coating with 100 nm thick Au layer, respectively.

images. Fig. 2(a–c) are schematic illustration whereas, Fig. 2(d) and 2(e) are the morphology of the Si NR arrays (diameter: 500 nm), before and after the electrode deposition. The Au coating was not restricted to the top of the Si NRs, and it also covered the individual NRs, which enabled the sensor to obtain the response from all the parts of the Si NRs during the pressure application.

Moreover, we investigated the pressure response of the Si NR-based pressure sensors when the pressure was applied through a mechanical approach via the VCM. A schematic illustration of the experimental setup is shown in Fig. 3(a). Fig. 3(b) shows the tilted image of the Si NR pressure sensor used to investigate the piezoresistive pressure response. The pressure sensing ability of the sensor manifested as a change in the conductivity during the pressure application. To clarify the sensitivity (S) and detection limit of the pressure range, we defined the response (R)

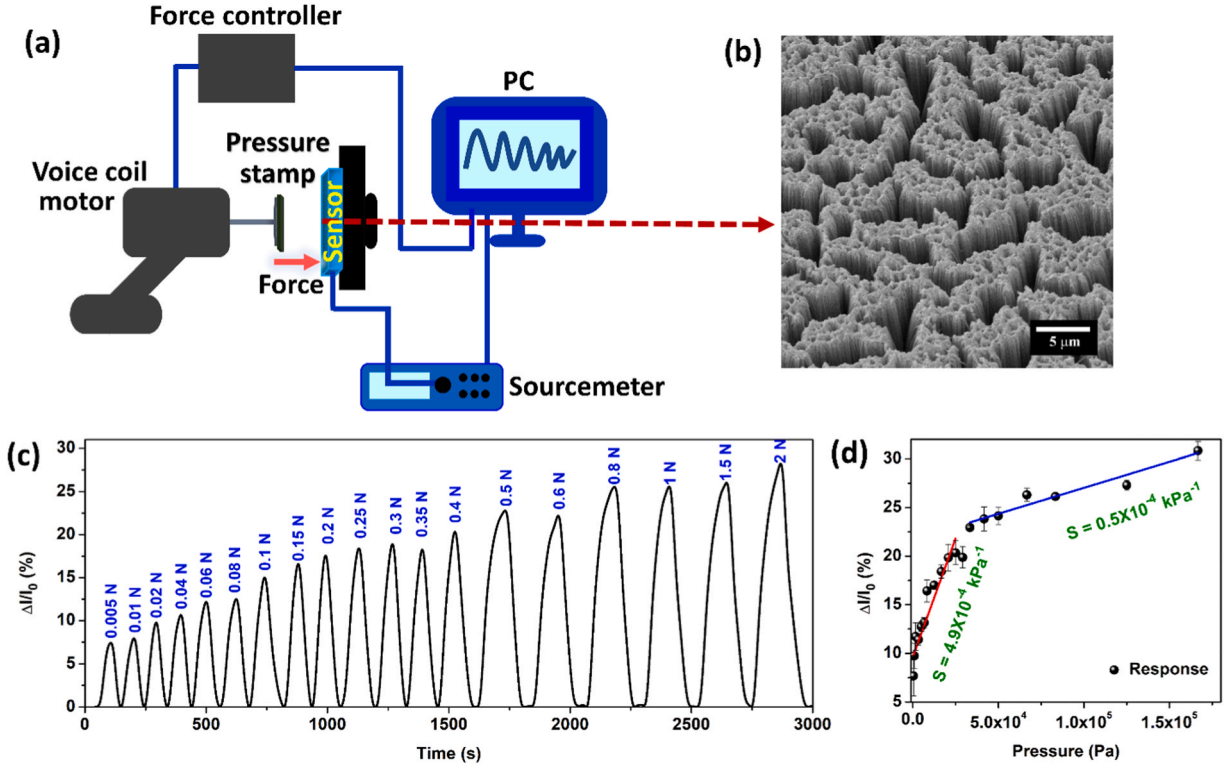

Fig. 3. Detection of pressure applied via mechanical force. (a) Schematic of the VCM setup to detect the mechanical pressure. (b) FESEM image of the sensor composed of Si NR arrays in NR_B. (c) Real-time pressure response of the Si NR sensor subjected to mechanical force by the VCM under fixed bias of 2 V. (d) Variation of the response of the sensor with the increase in the applied pressure. The solid line depicts the linear fit of the experimental data points.

and S of the sensor as follows:

$$R(\%) = \frac{\Delta I}{I_0}(\%) = \frac{I_{no\ pressure} - I_{pressure}}{I_{no\ pressure}} \times 100\ (\%), \quad (1)$$

$$S = \frac{\Delta R}{\Delta P}, \quad (2)$$

Where $I_{no\ pressure}$ and $I_{pressure}$ denote the current of the sensor in the absence and presence of pressure, respectively, and ΔR and ΔP indicate the relative change in the response and pressure, respectively. The real-time current response of the sensor under different applied forces is shown in Fig. 3(c), and 3(d) shows the current response of the sensor as a function of the applied pressure. An approximately linear relationship between the response and applied pressure can be observed in the range of 0–3 kPa, corresponding to a sensitivity of $S = 4.9 \times 10^{-4}$ kPa^{-1}. Beyond 3 kPa, the sensitivity decreases to $S = 5 \times 10^{-5}$ kPa^{-1}. Interestingly, the sensitivity is outperforming over that reported previously for an unconventional piezoresistive material Si having different structural configurations [26,29,33]. Note that in the existing studies, the Si NR-based sensors were cantilever type, with the electrodes installed at two different ends of an individual Si NR. In contrast, one electrode of the sensors in the present study was constructed by evaporating gold to the bundle of Si NR arrays from top, while the other one was common to the bottom. This configuration can improve the cumulative device performance by enhancing the load resistance and linearity in the response. Moreover, the sensor exhibited a high flexibility and did not break even after a pressure of 200 kPa was applied. In general, the current response of the pressure sensor corresponds to the pressure-induced change in the conductivity of the Si NRs via the piezoresistive effects. Although Si has a simple cubic structure, giant piezoresistive effects of Si NRs have been observed and it was explained by the change in the effective mass of the carriers [26]. Furthermore, various other approaches have been considered to explain the piezoresistive effects of Si NRs, among which, the quantum confinement (QC) effect and surface charge effect are the most popular and widely accepted [15,26–29,32]. Vinikman et al. reported that the piezoresistive response in Si NRs can be extended to Si by introducing pores on the Si NR surface, thereby interrupting the inherent symmetry [31]. According to the existing study results and our TEM analyses (Fig. 1(d–f)), we concluded that the chemically etched Si NRs in this study were highly porous, and the quantum-sized nano-size islands on the surface of the Si NRs were $< 111 >$-oriented [37,42]. The piezoresistive effect likely occurred owing to the QC of the e-h pairs in the quantum-sized Si nano-islands. Moreover, the symmetry of the Si atom ordering was disrupted in the Si nano-islands, as the bare Si wafer was $< 100 >$ oriented. According to He et al., the strain-induced changes in the mobility and effective mass of the carriers notably influence the piezoresistive properties of Si NRs [26]. The variance between the two different effective masses and mobilities is higher in the case of $< 111 >$ orientation compared to that in the $< 100 >$ orientation of Si, and hence, Si $< 111 >$ is more sensitive to the stress application [15,26,29,44]. Therefore, the chemically etched Si NRs can effectively respond to the pressure applied by different types of tools.

It was noted that the sensors exhibited a large response to the pressure when subjected to a constant flow of air. Fig. 4(a) shows the schematic of the experimental setup to clarify the current dynamic

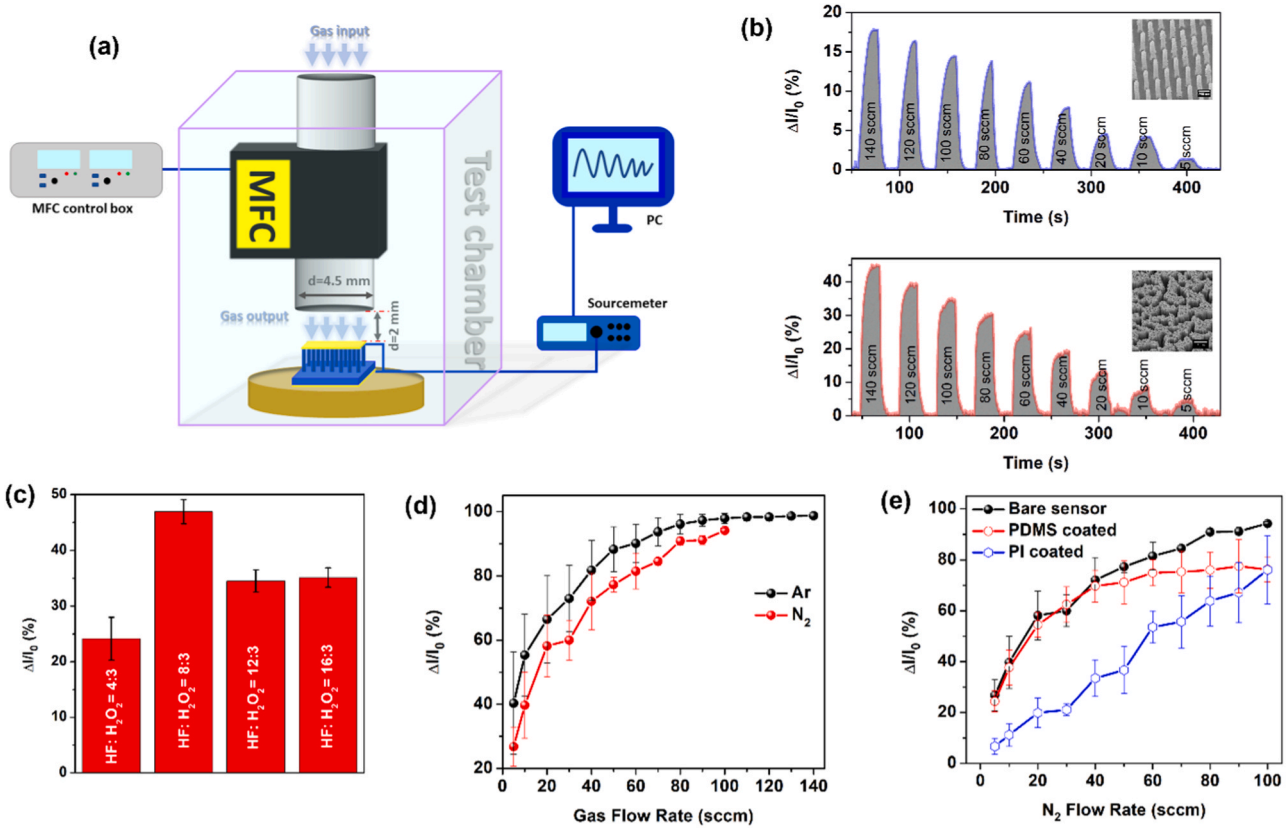

Fig. 4. Detection of pressure applied through a continuous gas flow. (a) Schematic of the experimental setup to detect the inert gas pressure. (b) Comparison of the real-time pressure responses from the NR_A (Si NR: diameter 200 nm, spacing 1 μm) and NR_B samples at different Ar gas flow rates. The sample size was 4 mm^2 in each case. The "flow on" mode is shaded in each case. The inset shows the corresponding FESEM image of the sensors. (c) Pressure response of the different Si NR samples prepared via 10 min etching under different etchant concentrations. The relative current change was measured at an Ar flow of 140 sccm with a sample size of 4 mm^2. (d) Comparison of pressure response of the NR_B sample with a sensor size of 16 mm^2, as a function of the gas flow rate for Ar and N_2. (e) Comparison of the pressure responses of the sensor before and after it was coated with a thin layer of polyimide and PDMS.

response of the sensor by introducing systematic variations in the inert gas flow. The Si NRs prepared using the two approaches, i.e., both the NR_A and NR_B samples, exhibited an excellent response to the extremely small Ar gas flow controlled precisely. Fig. 4(b) presents a comparison of the real-time pressure responses from the NR_A (diameter 200 nm, spacing 1 μm) and NR_B samples at different Ar gas flow rates. The sample size was 4 mm^2 in each case. The "flow on" mode is presented as the shaded region in each case. The inset shows the corresponding FESEM image of the sensors. In general, the gas flow on the Si NR surface can impart sufficient normal pressures that can deform the Si NR arrays and cause a relative change in the conductance due to the piezoresistive effect. Since the gas flow is turbulent inside the intermediate gaps of the Si NRs, it causes the Si NRs to vibrate, shake, and bend in multiple directions, thereby subjecting the Si nano-islands to a considerable stress. Note that the response is nearly three-fold larger in the case of NR_B samples, compared to that in the case of the 200 nm-diameter NR_A samples at all the flow rates. This phenomenon occurs because of the large particle density of the porous sites ($< 111 >$ sites) of the thin, close-packed Si NRs with the higher aspect ratio, that is, the NR_B samples. In contrast, the NR_A samples with a larger diameter do not bend easily in the case of the extremely small gas flow, compared to the NR_B samples. This phenomenon was observed by fabricating the sensor devices by using Si NRs with different diameters in the NR_A samples (as shown in Fig. S4(d)). However, the porosity, instead of the Si nano-island density on the Si NRs, plays a vital role in defining the piezoresistive response of the Si NRs. Hence, we tuned the porosity of the Si NRs by adjusting the etchant concentration during the preparation of the Si NRs (as shown in Fig. S2). The current response of the Si NRs with different porosities is shown in Fig. 4(c), and it can be noted that the piezoresistive response decreases with the decrease in the porosity. The Si NR prepared with a 4:3 HF/H_2O_2 concentration corresponds to the maximum porosity; nevertheless, the response is smaller in this case because of the smaller aspect ratio compared to that in the case of the other considered etchant concentration. The highest aspect ratio and porosity of the Si NRs occurred when the HF/H_2O_2 concentration was 8:3, and hence, these Si NRs were utilized for the practical application, as discussed in the subsequent sections. Moreover, the pressure response of the Si NRs depends on the effective sensor size. It was noted that the sensors having a size greater than or equal to 16 mm^2 exhibited the maximum response to the gas flow. In such cases, the cumulative deformation of the Si NRs is sufficient to exhibit a significant change in the current even for a small flow of the inert gas. Fig. S5 shows the real-time response of the sensor with a sensor size of 16 mm^2 under different Ar gas flow rates. The sensor exhibited a significant response (44.5%) even at the ultra-low flow of the Ar gas (5 sccm) and the response was nearly saturated at a flow rate of 100 sccm. The sensors were further tested to investigate the effect of different gases, and Fig. 4(d) shows the comparison of the response as a function of the gas flow rate for Ar and N_2. In both the gas flow cases, the trend was similar i.e., the response increased rapidly with the increase in the flow rate and became saturated after a certain value. In the case of the Ar gas flow, the response was ~95% at the flow rate of 100 sccm, beyond which it saturated. Since Ar has larger molar mass than N_2, Ar imparts higher pressure in each SCCM as compared to N_2. Hence, we obtained slightly higher pressure response from the sensor in Fig. 4(d) in case of Ar flow as compared to N2 flow. To avoid the effect of interfering components such as the humidity and adsorption of gases within the porous sites of the Si NRs, we coated the sensor device with a thin layer of polymer (PDMS as well as polyimide (PI)). Fig. 4(e) shows a comparison of the current response of the bare sensor with different polymer-coated sensors. After the polymer coating, the response of the sensor decreased, as expected. Note that the decrease in the performance usually depends upon the thickness of the respective polymer as well as its hardness; however, the polymer coating extends the longevity of the devices. Peng et al. examined the sensing property of porous Si NRs, which is a result of the charge transfer effect from a foreign molecule to the host material through the surface functional groups [45]. In the present context, we used the inert gases to impart pressure, and hence, the occurrence of such a phenomena were unlikely. For further verification, we modified the Si NRs through reactive ion etching (RIE) at $CF_4 = 45$ sccm and $Ar = 5$ sccm for different etching times. The pressure responses of the RIE-treated Si NR sensors were compared, as shown in Fig. S6. The RIE-treated samples exhibited a lower response, and the decrement in the pressure response further increased for the samples with prolonged RIE time. This phenomenon likely occurred because of the partial decrease in the surface porosity of the Si NRs. Hence, it can be considered that the pressure response of the Si NRs is due to the atomic-disorder-induced piezoresistivity, which originates at the quantum size Si nano-islands on the Si NR surface.

The MACE-prepared Si NRs could likely be used to detect the ultra-low pressure corresponding to the extremely small gas flow. Moreover, the sensors exhibited an excellent response to the gas flow even when operated at a considerably low power of 0.8 mW, as shown in Fig. S7(b). In addition, the sensor exhibited a considerably high response rate and excellent air stability (> 3 months and 1,000 cycles), as shown in Fig. S7(c) and (d), respectively. Almost no change was observed in the performance of the sensor after $> 1{,}000$ cycles. The reliable pressure response in an ambient atmosphere can ensure the high performance of the sensor in long-term use. Thus, these pressure sensor arrays can be applied in high-resolution electronic skin and other electronic devices.

Owing to its significant response at an extremely small gas flow and high sensitivity, the developed sensor can help to investigate the human breathing and monitor the respiratory status through the prototype sensor devices. Monitoring the human breath pattern is a noninvasive and sustainable monitoring method that can help diagnose pulmonary diseases at an early stage. The prototype Si NR-based pressure sensors can detect airflows under 5 sccm, which generate pressures with magnitudes less than 1 Pa. Therefore, the human breathing pattern was investigated through the sensors by attaching the sensor onto the philtrum of an individual, as shown in Fig. 5(a). Fig. 5(b) shows the pressure response in the periodic monitoring of the human breath. The sensor can efficiently detect the difference between the normal breathing (NB) and the states of hold breathing/stop breathing (SB) for some moments. Note that the continuous waveform during the NB can be assumed as a "normal" state of breathing, while its discontinuity corresponds to a potential "threat". The significant difference between the "normal" and "threat" conditions in Fig. 5(b) indicates that the sensor can provide an alarm in the case of risky events for an individual with breathing disorders such as sleep apnea. Fig. 5(c) shows the comparison of the effect of a physical workout on real-time breath patterns. Before and immediately after the exercise, the respiration frequencies are 22 and 41 per minute, respectively. Moreover, the breathing depth decreases after the exercise because of the high breathing rate compared to the response time. These results indicate to obtain more oxygen while exercising, we must reduce the breath rate and increase the breathing depth. The sensing performance of the sensor gradually decreased when it was used for continuous breathing. Note that the human breath is highly complex, owing to the presence of more than 800 compounds, which can interfere with the breath detection abilities of the Si NR-based sensors. The interfering agents present in the human breath, such as moisture and ammonia, are primarily responsible for the deteriorated performance of the sensor when used for an extended time. We performed the breath detection experiment for multiple cycles and after each cycle, the sensor was dehydrated. Fig. S8 (a–e) compares the breath sensing performance of the prototype sensor for 5 different cycles. The sensing performance was retained after each cycle and even more consistent in some cases than the bare one. Polymer coating is one of the well-accepted strategy for protecting devices to absorb moisture as the practical devices work in ambient condition. We coated the sensor with PI and the sensor was tested again for detecting human breath pattern. The breath sensing performances of PI-coated sensors are shown in Fig. S8(f) for thin PI S8 (g) for thick PI coating, respectively. The consistency in device

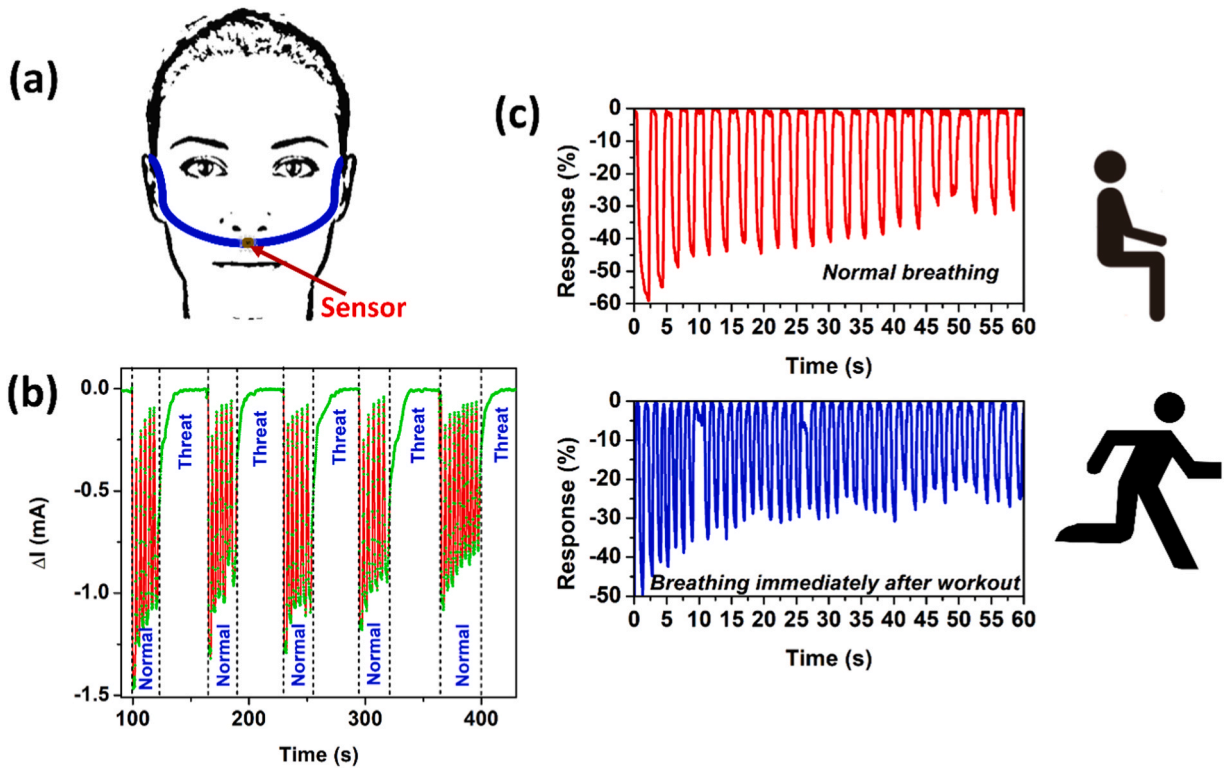

Fig. 5. Human breath detection. (a) Schematic of breath detection, indicating the sensor's placement on the philtrum. (b) Pressure response for NB and intermittent breathing (threat) condition in a regular interval. (c) Comparison of breathing pattern before (upper panel) and after (lower panel) a physical workout.

performance was increased after PI covering and further enhanced by increasing PI thickness. However, there was a considerable compromise in devices sensitivity.

Owing to the excellent breath-sensing performance, biocompatibility and air stability of the well-established CMOS-compatible nanomaterial, the Si NR-based piezoresistive sensors were considered for use in next-generation breath monitoring devices. Fig. 6(a) shows the integration of the sensors with a Bluetooth/Wi-Fi-based module. In particular, the sensor was attached on a flexible PCB and placed on the philtrum, as shown in Fig. 6(b). Arduino ESP-32 was used to operate and accumulate the breathing waveform, which was further recorded by a smartphone/computer (Fig. 6(c)). The circuit diagram of the complete setup is shown in Fig. 6(d). The setup was designed to realize a portable and wearable platform for the sensor that can inconspicuously fit in our everyday life. The sensor can monitor the breath signal continuously and detect the abnormalities/disorders in the human respiratory system. In real life applications, a major concern is to identify whether babies are able to breath properly during sleep. Fig. 6 (e) shows the real-time waveform of the breath signals recorded by the sensor with the conditions switched between NB and SB. The corresponding movie is provided as "Supplementary video I". The findings indicate that the sensor can be used as a sleep partner to ensure smooth breathing during the sleep time. In addition, by distinguishing the difference between the NB and breathing in harsh conditions, one can detect different types of diseases related to the human respiratory system, such as tachypnea (abnormally rapid breathing), asthma, and chronic bronchitis (chronic obstructive pulmonary disease).

Supplementary material related to this article can be found online at . doi:10.1016/j.nanoen.2020.105537.

At present, many people are incorporating daily workouts in their lives, owing to its necessity in the modern lifestyle to maintain health and fitness. Consequently, it is desirable to frequently monitor such workouts. Fig. 6(f) shows the real-time waveform of the breath signals recorded by the sensor under normal and running conditions periodically. The corresponding movie is provided as "Supplementary video II". It can be noted that the breathing rate is low and stable during rest and high and frequent during running, as expected. Thus, the Si NR-based sensor can be utilized as an exercise counter and motivator for a physical fitness enthusiast in parallel with the highly popular pedometer. Furthermore, as humans age, the capability of the body in undertaking strenuous exercises reduces. During workout/jogging, especially for an elderly person, the proposed sensor can provide alarms in the case of extra-fast, frequent and abnormal breathing to prevent any critical conditions. The prototype sensor works consistently in an ambient condition, indicating its potential to be implemented in next-generation breath sensors.

Supplementary material related to this article can be found online at . doi:10.1016/j.nanoen.2020.105537.

These findings highlight a novel opportunity to fabricate technology-compatible, dimension- and position-controlled pressure sensor arrays in an easy yet inexpensive way and its versatile cutting-edge applications interfacing with different electronic devices.

4. Conclusions

This study was aimed at demonstrating a bio-compatible, large-area, simple, easy, rapid, scalable and controlled fabrication of highly sensitive pressure sensors by using chemically etched Si NR arrays. The introduction of quantum-sized Si nano-islands and disrupting the symmetry in the atomic ordering on the Si NR surface can help realize a superior piezoresistive response in chemically etched Si NR arrays. The piezoresistive property of Si NR arrays, incorporated from both the position and dimension-controlled etching as well as random etching, is exploited to develop a pressure sensor to detect different mechanical forces with considerable sensitivity. The high sensitivity at an extremely small air flow enables the pressure sensor to monitor the human respiration by precisely tracking the rate and depth of breathing. Moreover, we successfully demonstrated the development of a portable and

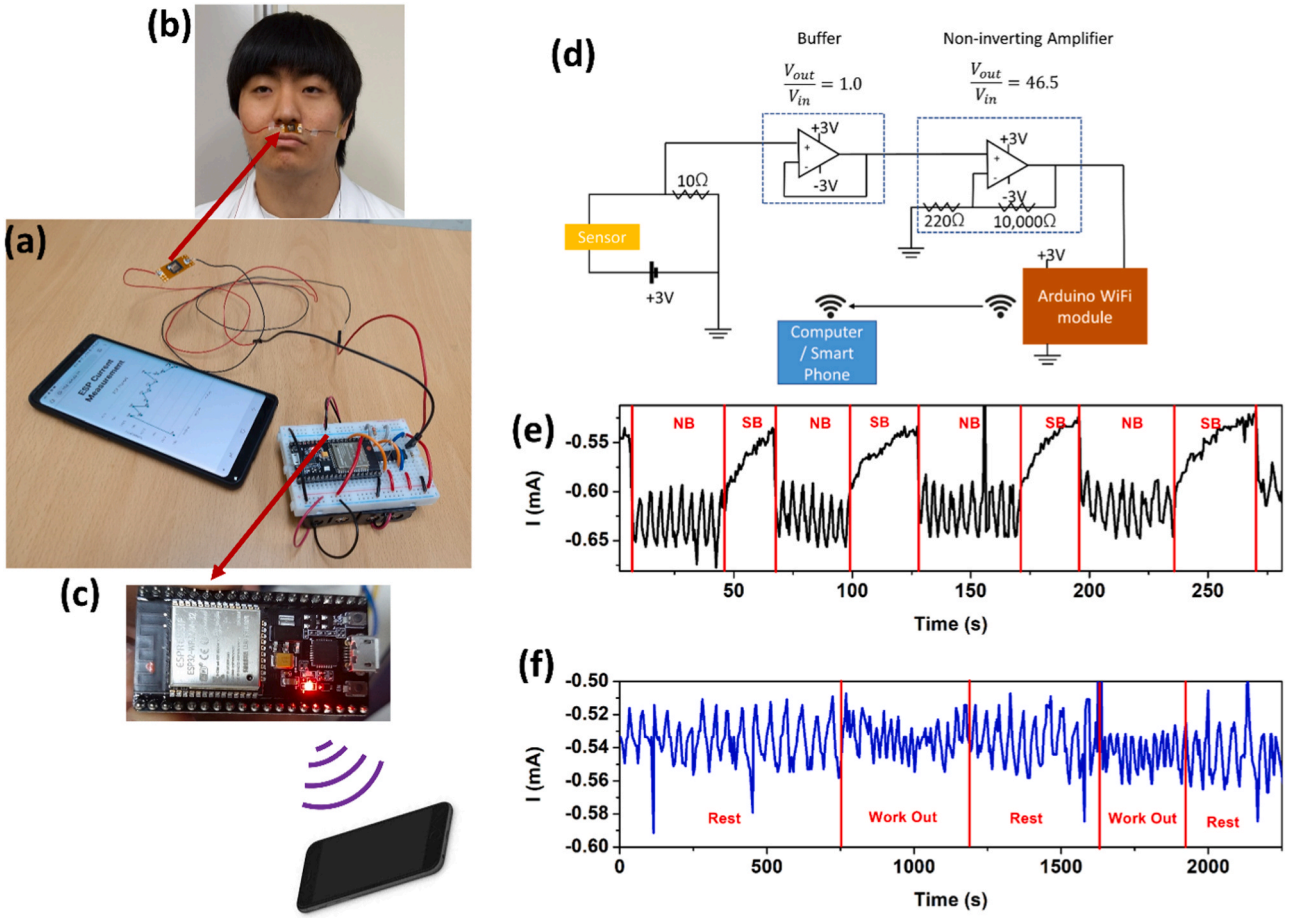

Fig. 6. Portable breath sensor. (a) Digital photograph of the portable breath sensor integrated with a Bluetooth-based module (Arduino ESP-32). (b) The sensor attached with the flexible PCB was placed on the philtrum. The effective sensor size was 9 μm^2. (c) Bluetooth/WiFi-based module (Arduino ESP-32) integrated with the wireless gadget. (d) Circuit diagram of the portable breath sensor. (e) Pressure response for the NB and SB (blocked by obstacle) conditions at a regular interval. (f) Comparison of the breathing during rest and a minor workout.

wearable breath sensor to monitor the respiratory parameters in a noninvasive and personalized manner. Wireless integration of the sensors, having the portable and smart platform, can enhance the utility of the breath sensor as a routine-life workout partner and can be considered to realize next-generation breath-sensing gadgets. We believe that this work provides guidance to develop next-generation breath-sensing gadgets and other leading-edge applications in electronic and healthcare devices.

CRediT authorship contribution statement

Ramesh Ghosh: Writing - original draft, Conceptualization, Methodology, Investigation, Data curation, Formal analysis. **Minho S. Song:** Investigation, Writing - review & editing. **Junbeom Park:** Investigation. **Youngbin Tchoe:** Investigation. **Puspendu Guha:** Investigation, Formal analysis, Writing - review & editing. **Wanhee Lee:** Investigation, Designing computer programs. **Yoonseo Lim:** Investigation, Writing - review & editing. **Bosung Kim:** Investigation, Validation. **Sang-Woo Kim:** Investigation, Validation. **Miyoung Kim:** Investigation, Validation. **Gyu-Chul Yi:** Writing - original draft, Formal analysis, Conceptualization, Project administration, Funding acquisition.

Declaration of Competing Interest

The authors declare that they have no known competing financial interests or personal relationships that could have appeared to influence the work reported in this paper.

Acknowledgments

We acknowledge the Brain Korea 21-Plus Program and Institute of Applied Physics, Seoul National University for providing the financial support to conduct part of this work. In addition, this work was supported by the Samsung Research Funding Center of Samsung Electronics (SRFC-TA1803-02(0417-20180116)).

Appendix A. Supporting information

Supplementary data associated with this article can be found in the online version at doi:10.1016/j.nanoen.2020.105537.

References

[1] Z.L. Wang, J. Song, Piezoelectric nanogenerators based on zinc oxide nanowire arrays, Science 312 (2006) 242–246.
[2] T.Q. Trung, N.-E. Lee, Flexible and stretchable physical sensor integrated platforms for wearable human-activity monitoringand personal healthcare, Adv. Mater. 28 (2016) 4338–4372.
[3] A.T. Güntner, S. Abegg, K. Königstein, P.A. Gerber, A. Schmidt-Trucksäss, S. E. Pratsinis, ACS Sens. 4 (2019) 268–280.
[4] J.S. Floras, Sleep apnea and cardiovascular disease: an enigmatic risk factor, Circ. Res. 122 (2018) 1741–1764.
[5] B.C.K. Tee, C. Wang, R. Allen, Z. Bao, An electrically and mechanically self-healing composite with pressure- and flexion-sensitive properties for electronic skin applications, Nat. Nanotechnol. 7 (2012) 825–832.
[6] S. Gong, W. Schwalb, Y. Wang, Y. Chen, Y. Tang, J. Si, B. Shirinzadeh, W. Cheng, A wearable and highly sensitive pressure sensor with ultrathin gold nanowires, Nat. Commun. 5 (2014) 3132.

[7] C.H. Hu, C.H. Liu, L.Z. Chen, Y.C. Peng, S.S. Fan, Resistance-pressure sensitivity and a mechanism study of multiwall carbon nanotube networks/poly (dimethylsiloxane) composites, Appl. Phys. Lett. 93 (2008), 033108.
[8] J. Li, R. Bao, J. Tao, Y. Peng, C. Pan, Recent progress in flexible pressure sensor arrays: from design to applications, J. Mater. Chem. C 6 (2018) 11878–11892.
[9] W.S. Su, Y.F. Chen, C.L. Hsiao, L.W. Tu, Generation of electricity in GaN nanorods induced by piezoelectric effect, Appl. Phys. Lett. 90 (2007), 063110.
[10] Y.-F. Lin, J. Song, Y. Ding, S.-Y. Lu, Z.L. Wang, Piezoelectric nanogenerator using CdS nanowires, Appl. Phys. Lett. 92 (2008), 022105.
[11] Z. Zhao, X. Pu, C. Han, C. Du, L. Li, C. Jiang, W. Hu, Z.L. Wang, Piezotronic effect in polarity-controlled GaN nanowires, ACS Nano 9 (2015) 8578–8583.
[12] B. Su, S. Gong, Z. Ma, L.W. Yap, W. Cheng, Mimosa-inspired design of a flexible pressure sensor with touch sensitivity, Small 11 (2015) 1886–1891.
[13] B. Zhu, Z. Niu, H. Wang, W.R. Leow, H. Wang, Y. Li, L. Zheng, J. Wei, F. Huo, X. Chen, Microstructured graphene arrays for highly sensitive flexible tactile sensors, Small 10 (2014) 3625–3631.
[14] B. Zhu, Y. Ling, L.W. Yap, M. Yang, F. Lin, S. Gong, Y. Wang, T. An, Y. Zhao, W. Cheng, Hierarchically structured vertical gold nanowire array-based wearable pressure sensors for wireless health monitoring, ACS Appl. Mater. Interfaces 11 (2019) 29014–29021.
[15] A.S. Fiorillo, C.D. Critello, S.A. Pullano, Theory, technology and applications of piezoresistive sensors: a review, Sens. Actuators A Phys. 281 (2018) 156–175.
[16] K. Song, R. Zhao, Z.L. Wang, Y. Yang, Conjuncted pyro-piezoelectric effect for self-powered simultaneous temperature and pressure sensing, Adv. Mater. 31 (2019), 1902831.
[17] J. Sun, H. Guo, J. Ribera, C. Wu, K. Tu, M. Binelli, G. Panzarasa, F.W.M.R. Swarze, Z.L. Wang, I. Burgert, Surface-enhanced raman scattering trace-detection platform based on continuous-rolling-assisted evaporation on superhydrophobic surfaces, ACS Nano 3 (2020) 4767–4776.
[18] K.Y. Shin, J.S. Lee, J. Jang, Highly sensitive, wearable and wireless pressure sensor using free-standing ZnO nanoneedle/PVDF hybrid thin film for heart rate monitoring, Nano Energy 22 (2016) 95–104.
[19] C. Jin, N. Hao, Z. Xu, I. Trase, Y. Nie, L. Dong, A. Closson, Z. Chen, J.X.J. Zhang, Flexible piezoelectric nanogenerators using metal-doped ZnO-PVDF films, Sens. Actuators A Phys. 305 (2020), 111912.
[20] L. Dong, C. Jin, A.B. Closson, I. Trase, H.C. Richards, Z. Chen, J.X.J. Zhang, Cardiac energy harvesting and sensing based on piezoelectric and triboelectric designs, Nano Energy 76 (2020), 105076.
[21] R. Ghosh, P.K. Giri, Silicon nanowire heterostructures for advanced energy and environmental applications: a review, Nanotechnology 28 (2017), 012001.
[22] H. Han, Z. Huang, W. Lee, Metal-assisted chemical etching of silicon and nanotechnology applications, Nano Today 9 (2014) 271–304.
[23] Y. Qu, H. Zhoua, X. Duan, Porous silicon nanowires, Nanoscale 3 (2011) 4060.
[24] L. Baraban, B. Ibarlucea, E. Baek, G. Cuniberti, Hybrid silicon nanowire devices and their functional diversity, Adv. Sci. 6 (2019), 1900522.
[25] F. Priolo, T. Gregorkiewicz, M. Galli, T.F. Krauss, Silicon nanostructures for photonics and photovoltaics, Nat. Nanotechnol. 9 (2014) 19–32.
[26] R. He, P. Yang, Giant piezoresistance effect in silicon nanowires, Nat. Nanotechnol. 1 (2006) 42–46.
[27] J.S. Milne, A.C.H. Rowe, S. Arscott, C. Renner, Giant piezoresistance effects in silicon nanowires and microwires, Phys. Rev. Lett. 105 (2010), 226802.
[28] A. Lugstein, M. Steinmair, A. Steiger, H. Kosina, E. Bertagnolli, Anomalous piezoresistance effect in ultrastrained silicon nanowires, Nano Lett. 10 (2010) 3204–3208.
[29] K. Winkler, E. Bertagnolli, A. Lugstein, Origin of anomalous piezoresistive effects in VLS grown Si nanowires, Nano Lett. 15 (2015) 1780–1785.
[30] S. Zhang, L. Lou, C. Lee, Piezoresistive silicon nanowire based nanoelectromechanical system cantilever air flow sensor, Appl. Phys. Lett. 100 (2012), 023111.
[31] S. Vinikman-Pinhasi, E.N. Ribak, Piezoelectric and piezooptic effects in porous silicon, Appl. Phys. Lett. 88 (2006), 111905.
[32] A.C.H. Rowe, Silicon nanowires feel the pinch, Nat. Nanotechnol. 3 (2008) 311–312.
[33] A.C.H. Rowe, Piezoresistance in silicon and its nanostructures, J. Mater. Res. 29 (2014) 731–744.
[34] P. Neuzil, C.C. Wong, J. Reboud, Electrically controlled giant piezoresistance in silicon nanowires, Nano Lett. 10 (2010) 1248–1252.
[35] J. Park, Y. Lee, J. Hong, M. Ha, Y.-D. Jung, H. Lim, S.Y. Kim, H. Ko, Giant tunneling piezoresistance of composite elastomers with interlocked microdome arrays for ultrasensitive and multimodal electronic skins, ACS Nano 8 (2014) 4689–4697.
[36] U. Mogera, A.A. Sagade, S.J. George, G.U. Kulkarni, Ultrafast response humidity sensor using supramolecular nanofibre and its application in monitoring breath humidity and flow, Sci. Rep. 4 (2014) 4103.
[37] R. Ghosh, P.K. Giri, K. Imakita, M. Fujii, Origin of visible and near-infrared photoluminescence from chemically etched Si nanowires decorated with arbitrarily shaped Si nanocrystals, Nanotechnology 25 (2014), 045703.
[38] S.A. Kara, A. Keffous, A.M. Giovannozzi, A.M. Rossi, E. Cara, L. D'Ortenzi, K. Sparnacci, L. Boarino, N. Gabouze, S. Soukane, Fabrication of flexible silicon nanowires by self-assembled metal assisted chemical etching for surface enhanced Raman spectroscopy, RSC Adv. 6 (2016) 93649–93659.
[39] W.-K. To, C.-H. Tsang, H.-H. Li, Z. Huang, Fabrication of n-type mesoporous silicon nanowires by one-step etching, Nano Lett. 11 (2011) 5252–5258.
[40] R. Ghosh, A. Pal, P.K. Giri, Quantitative analysis of the phonon confinement effect in arbitrarily shaped Si nanocrystals decorated on Si nanowires and its correlation with the photoluminescence spectrum: Quantitative analysis of the phonon confinement effect in arbitrarily shaped Si nanocrystals, J. Raman Spectrosc. 46 (2015) 624–631.
[41] C. Chiappini, X. Liu, J.R. Fakhoury, M. Ferrari, Biodegradable porous silicon barcode nanowires with defined geometry, Adv. Funct. Mater. 20 (2010) 2231–2239.
[42] W. Chern, K. Hsu, I.S. Chun, B.Pd Azeredo, N. Ahmed, K.H. Kim, J.-m Zuo, N. Fang, P. Ferreira, X. Li, Nonlithographic patterning and metal-assisted chemical etching for manufacturing of tunable light-emitting silicon nanowire arrays, Nano Lett. 10 (2010) 1582–1588.
[43] C. Romanitan, P. Varasteanu, I. Mihalache, D. Culita, S. Somacescu, R. Pascu, E. Tanasa, S.A.V. Eremia, A. Boldeiu, M. Simion, A. Radoi, M. Kusko, High-performance solid state supercapacitors assembling graphene interconnected networks in porous silicon electrode by electrochemical methods using 2,6-dihydroxynaphthalen, Sci. Rep. 8 (2018) 9654.
[44] T. Barwicz, L. Klein, S.J. Koester, H. Hamann, Silicon nanowire piezoresistance: Impact of surface crystallographic orientation, Appl. Phys. Lett. 97 (2010), 023110.
[45] K.-Q. Peng, X. Wang, S.-T. Lee, Gas sensing properties of single crystalline porous silicon nanowires, Appl. Phys. Lett. 95 (2009), 243112.

Ramesh Ghosh received his Ph.D. degree in Physics in 2017 from Indian Institute of Technology Guwahati, India. He received an offer of Brain Korea 21-Plus from South Korea and worked under Prof. Gyu-Chul Yi in Seoul National University as a postdoctoral researcher. After spending 2.5 years in Seoul National University, he moved to his current work place, University of Glasgow, United Kingdom, where he is appointed as a research associate under Prof. Nikolaj Gadegaard. His research interest is focused on the ordered array of 1D nanostructures and its heterostructures for optoelectronic and bio-physical applications.

Minho S. Song obtained his Ph.D. degree in physics from Seoul National University in 2020. Currently, he is working as a postdoc in physics department at Seoul National University from 2020. His research focuses on the biomedical applications using semiconductor nanomaterials and growth of semiconductor nanomaterials using metal-organic chemical vapor deposition (MOCVD).

JunBeom Park obtained his Ph.D. degree in physics from Seoul National University in 2018. Currently, he is working in Samsung Electronics Co., Ltd. from 2018. He contributed in research in the field of semiconductor nanomaterial growth using metal-organic chemical vapor deposition(MOCVD) and nanodevice fabrication for pressure sensor.

Youngbin Tchoe received his B.S. degree (2011) and Ph.D. degree (2018) in Physics from Seoul National University, Seoul, Korea, under supervision of Prof. Gyu-Chul Yi. Currently, he is a postdoctoral fellow in the Department of Electrical and Computer Engineering at University of California, San Diego, La Jolla, USA, working with Prof. Shadi A. Dayeh.

Puspendu Guha received his Ph.D. degree in Physics from Homi Bhabha National Institute, India in 2018. Currently, he is a postdoctoral researcher at Seoul National University, Republic of Korea. His current research interest is fabrication and electron microscopy characterization of 2D heterostructures and their device applications.

Wanhee Lee has been an undergraduate student majoring in physics at Seoul National University since 2014. His interest ranges from the fundamental understanding of electronic and optical properties of low-dimensional materials to the high-quality material design and synthesis for novel device applications.

Yoonseo Lim is an undergraduate student in Imperial College London. As a part of the Material Science and Engineering Degree, she takes interest in a variety of subjects; from the different origins of piezoresistivity in materials to the growth of inorganic rods on 2D substrates. Her current enthusiasm lies in the use of multi-physics software and computing languages to hypothesize and simulate the outcome of experiments.

Bosung Kim is a Ph.D. student under the supervision of Prof. Sang-Woo Kim at School of Advanced Materials Science & Engineering, Sungkyunkwan University (SKKU). His current research is fabrication and characterization of piezoelectric and triboelectric nanogenerators for energy harvesting and their applications in wearable devices and biomedical engineering.

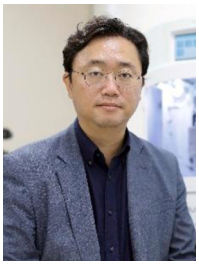

Sang-Woo Kim is a full professor in the Department of Advanced Materials Science and Engineering at Sungkyunkwan University (SKKU). His recent research interest is focused on piezoelectric/triboelectric nanogenerators, photovoltaics, and 2D materials including graphene, MoS2 etc. Now he is a director of SAMSUNG-SKKU Graphene/2D Research Center and is leading National Research Laboratory for Next Generation Hybrid Energy Harvester. He was the Conference Chair of the 4th NGPT (Nanogenerator Piezotronics) in 2018.

Miyoung Kim is a full professor in the Department of Materials Science and Engineering at Seoul National University, Republic of Korea. She received her Ph.D. degree in Physics from Arizona State University, USA in 1998. Prof. Kim was a postdoctoral researcher in Oak Ridge National Laboratory for three years (1998–2001). She joined Seoul National University in 2004. Prof. Kim's current research interests include quantitative interpretation of single atomic imaging and spectroscopy and relating atomic and electronic structures of nano-materials to physical properties.

Gyu-Chul Yi is a professor in the Department of Physics at Seoul National University. He received Ph.D. degree (1997) from Northwestern University. After working as postdoctoral researcher at Oak Ridge National Laboratory, he joined Pohang University of Science and Technology, Korea in 1999 as an assistant professor. Since 2004, he has been director of the National CRI Center for Semiconductor Nanostructures. He has extensive experience in wide-bandgap semiconductor nanostructures and has published more than 250 referred articles in Science, Advanced Materials, Nano Letters, Nano Energy, etc. He has also written books as an editor and several book chapters as author/coauthor.